Article

Effect of Secondary Structures on the Adsorption of Peptides onto Hydrophobic Solid Surfaces Revealed by SALDI-TOF and MD Simulations

Young Hyun No, Nam Hyeong Kim, Muhammad Shahzad Zafar, Seon Hwa Park, Jaecheol Lee, Heeyeop Chae, Wan Soo Yun,* Young Dok Kim,* and Yong Ho Kim*

Read Online

ACCESS | Metrics & More | Article Recommendations | Supporting Information

ABSTRACT: The adsorption of peptides and proteins on hydrophobic solid surfaces has received considerable research attention owing to their wide applications to biocompatible nanomaterials and nanodevices, such as biosensors and cell adhesion materials with reduced nanomaterial toxicity. However, fundamental understandings about physicochemical hydrophobic interactions between peptides and hydrophobic solid surfaces are still unknown. In this study, we investigate the effect of secondary structures on adsorption energies between peptides and hydrophobic solid surfaces via experimental and theoretical analyses using surface-assisted laser desorption/ionization-time-of-flight (SALDI-TOF) and molecular dynamics (MD) simulations. The hydrophobic interactions between peptides and hydrophobic solid surfaces measured via SALDI-TOF and MD simulations indicate that the hydrophobic interaction of peptides with random coil structures increased more than that of peptides with an α-helix structure when polar amino acids are replaced with hydrophobic amino acids. Additionally, our study sheds new light on the fundamental understanding of the hydrophobic interaction between hydrophobic solid surfaces and peptides that have diverse secondary structures.
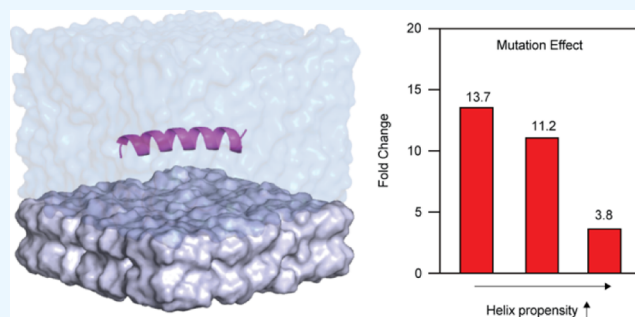
INTRODUCTION

The study on hydrophobic interactions of peptides on inorganic surfaces is critical in the field of materials science. Recently, based on the knowledge of these interactions, several adaptable biocompatible materials have been developed for use in biosensors.[1−4] Moreover, novel materials can be realized using these interactions for applications, such as antimicrobial efficiency,[5] water treatment,[6] and biomedical application.[7−9] Due to its ever-increasing application, several researchers have tried to understand the effects of several factors on the adsorption of proteins/peptides onto hydrophobic surfaces, namely, solution pH, temperature, molecular weight, isoelectric point, and chemical properties.[10−14] However, not only the peptide sequence but also the secondary structure, along with the surface properties, such as topography, roughness, and surface chemistry, plays a key role when a peptide is docked onto a hydrophobic surface.[15−21] For the effective stabilization of a protein, the effect of the presence of a physical surface plays a key role in reducing the entropy of the unfolded state.[22−26] To address this aspect, researchers have studied the interactions to adsorption on a solid surface using naturally existing proteins, such as BSA,[27] lysozyme,[28] and peptide-like PLL.[25] The common rationale for their selection was a specific type of protein or peptide with inherent mixed structures of α-

helix and β-sheets, which limits the scope of the study. Furthermore, there are controversial discussions related to the effect of secondary structures for interaction with hydrophobic surfaces. Some researchers observed that α-helix represented more robust structural properties for interaction with hydrophobic surfaces than β-sheets in lysozymes.[29] In contrast, some researchers studied that β-sheets were stiffer structural units compared to α-helix on the graphene surface.[30] For better understanding of the structure and dynamics of interfacial peptides, experimental techniques such as vibrational sum frequency generation spectroscopy have also been developed.[31,32] However, the effect of a random coil structure for hydrophobic interactions and how the interactions can be modulated when the sequence is changed with specific secondary structures are still largely unknown.

In this paper, we report the effect of secondary structures on hydrophobic interactions between peptides and hydrophobic solid surfaces with experimental and theoretical analyses using surface-assisted laser desorption/ionization-time-of-flight (SALDI-TOF) and molecular dynamics (MD) simulations. The peptides were modulated by adjusting the number of amino acids to observe the effect of secondary structures on hydrophobic interactions when the peptide sequence is mutated from polar amino acids to hydrophobic amino acids. Specifically, we increased the α-helix structural stability by extending the length of peptides and the hydrophobicity of peptides mutating polar amino acids (E; glutamic acid) into hydrophobic amino acids (I; isoleucine). To measure the hydrophobic interactions between peptides and hydrophobic solid surfaces, we designed an inorganic matrix that can be used to measure hydrophobic interactions with SALDI-TOF principle using polydimethylsiloxane (PDMS)-coated TiO$_2$ nanoparticles. Subsequently, to calculate the peptide-PDMS binding energy when modulated peptides bind to PDMS, we performed MD simulations. Our results showed that the mutations in peptides with a random coil structure are more effective in hydrophobic interactions with PDMS than mutations in peptides with an α-helix structure.

■ METHODS

Peptide Synthesis. The peptide candidates were synthesized by the Fmoc chemistry-based H-Rink amide ChemMatrix resin (0.1 mmol, 14 synthesis scale, 0.53 mmol/g substitution value, PCAS BioMatrix Inc.) by a manual solid-phase peptide synthesizer. Before starting the synthesis, the resin was swelled in N,N-dimethylformamide (DMF) for 30 min. The Fmoc amino acid was deported by the deprotecting solution (piperidine 20% and DMF 80%) and coupled with the activated amino acid (HBTU and DIEA) at 75 ± 5 °C for 5 and 7 min, respectively, with alternating steps of washing with DMF and dichloromethane three times after every deprotecting and coupling step. The different lengths of PBP-7aa, PBP-14aa, and PBP-21aa were cleaved from the solid support by the cleavage solution containing trifluoroacetic acid (TFA)/triisopropylsilane/H$_2$O (95:2.5:2.5). At room temperature, the solution was stirred for 2 h. After stirring, the cleavage solute was filtered for separation from the resin, and the solvent was evaporated under the flow of N$_2$ gas. Afterward, the crude peptides were precipitated in cold diethyl ether and lyophilized with powder.

Peptide Purification and Confirmation of Mass. The PBP peptide candidates were purified on high-performance liquid chromatography (HPLC, Agilent) by using a C4 column (Agilent) in mobile-phase solutions of A (100% DI water and 0.1% TFA) and stationary-phase solutions of B (90% ACN, 10% distilled water, and 0.1% TFA). The gradients were set at 10% during 10 min, 70% during 70 min, and 100% during 75 min 10%——80 min with a 1%/min rate. The molecular mass of all peptides was confirmed by matrix-assisted laser desorption/ionization-time-of-flight (MALDI-TOF) mass spectrometry using a Bruker Micro Ultra flex III mass spectrometer (flex control 1.01).

Preparation of PDMS-Coated TiO$_2$ Nanoparticles. The TiO$_2$ nanoparticles coated with PDMS were synthesized by the thermal deposition method. The PDMS-coated TiO$_2$ surface was characterized using FT-IR adsorption spectra (Vertex 70 series, Bruker Korea) and subjected to test at a 4 cm^{-1} resolution. The X-ray diffraction patterns of bare TiO$_2$ and

PDMS-coated TiO$_2$ surfaces were recorded on a diffractometer. For the optical absorption arrangement of bare TiO$_2$ and PDMS-coated TiO$_2$ nanoparticles, the ultraviolet−visible (UV−vis) absorption spectra of both samples were obtained in the reflection mode. The matrix solutions for SALDI-TOF measurements were prepared by dispersing 0.05 g of bare TiO$_2$ or PDMS-coated TiO$_2$ nanoparticle powder in 10 mL of 99% ethanol. Each solution was bath-sonicated for 90 min at 100% power. The solution was placed overnight, and a supernatant was selected to be used as the SALDI-TOF matrix.

Measurement of SALDI-TOF. SALDI-TOF MS measurements were performed in positive-ion and reflection modes by using an Ultra flex III mass spectrometer (Bruker Daltonics) equipped with a 337 nm pulsed nitrogen laser. The applied acceleration voltage was +20 kV to obtain high resolution and high signal-to-noise (S/N) ratio; each mass spectrum was generated by an average of 200 laser pulses. We measured the same spot five times to obtain the average and standard deviation of the intensity. The signal intensity of SALDI-TOF MS was obtained at 30% of maximum laser power by using the CHCA organic matrix and 40% of maximum laser power when using the TiO$_2$ matrix and the PDMS-coated TiO$_2$ matrix. Data processing was performed with the Flex analysis 3.0 software.

MD Simulations. To simulate the molecular adsorption of PBP peptide candidates on the PDMS surface, we carried out all-atom MD simulations with explicit water by using the NAMD package with the CHARMM36m force field.[33] The initial structure is constructed with PDMS and peptides whose secondary structure is known as a helix reported in the protein data bank (PDB) with a PDB code of 3S0R. The peptide sequences were truncated and mutated to understand the effects of the secondary structure to the hydrophobic interaction. The force field parameters of PDMS were added based on a previous research.[17,34] To construct a PDMS substrate, we first pre-equilibrated a single chain of PDMS for 10 ns. We extracted 12 conformations of PDMS on the last 2.4 ns trajectory with an interval of 200 ps, and they were positioned in a layer into a plate of 50 × 50 × 13 Å^3 to construct a stable PDMS substrate. We performed equilibrium MD simulations of a layer PDMS with explicit water using periodic boundary conditions for 10 ns. The modulated peptide candidates were positioned on top of the PDMS substrate with a height of 5 Å. An explicit solvent box was constructed with a TIP3P water model. After 10^3 energy minimization steps, the equilibrium dynamic simulation was implemented based on the NPT ensemble at 310 K for 500 ns. The time step was 2 fs/step for rigid bond simulation, and the trajectory was recorded every 10 ps. The binding energies between the peptide and PDMS surface was calculated with the molecular mechanics-Poisson−Boltzmann surface area (MM-PBSA) method. MM-PBSA is described as

$$\Delta G_{\text{bind}} = \Delta E_{\text{MM}} + \Delta G_{\text{np}} + \Delta G_{\text{PB}}$$

where ΔE_{MM} is the molecular mechanics energy, ΔG_{np} is the nonpolar solvation energy, and ΔG_{PB} is the polar solvation energy. The entropy contribution can be omitted due to the relative binding energy. When we want to calculate the relative binding energies of some peptides that have a similar structure and binding modes, the entropy contribution can be omitted. We calculated only ΔE_{MM}, ΔG_{np}, and ΔG_{PB} energies.

Table 1. In the same sequence, the structure was controlled by change in length by mutating the charged residue (E, Glu) to a hydrophobic residue (I, Ile), and mutation is performed once per seven residues[a]

Peptide Name	Sequence	MW	Hydrophobicity	Secondary Structure
HexCoil-Ala-Native	AEAESALEYAQQALEKAQLALQAARQALKA			
1. PBP-7aa-Nat	EKAQLAL	813.0	0.043	Random Coil
2. PBP-7aa-Mut	IKAQLAL	797.0	1.186	Random Coil
3. PBP-14aa-Nat	EYAQQALEKAQLAL	1616.8	-0.293	α-Helix / Coil
4. PBP-14aa-Mut	IYAQQALIKAQLAL	1584.9	0.850	α-Helix / Coil
5. PBP-21aa-Nat	AEAESALEYAQQALEKAQLAL	2288.5	-0.129	α-Helix
6. PBP-21aa-Mut	AEAISALIYAQQALIKAQLAL	2240.6	1.014	α-Helix

[a]Comparison was proceeded for two peptides, which have the same difference of hydrophobicity (1.143).

RESULTS AND DISCUSSION

Modulation of Peptides Varying Secondary Structure and Hydrophobicity. To understand the effect of the secondary structure of the peptide on its adsorption onto a hydrophobic surface, the peptide candidates were constructed for controlling the structural stability of α-helix and hydrophobicity of peptides (Table 1). From the same sequence of a peptide with α-helix secondary structure, the structural stability was controlled by a change in the number of amino acids. As the number of amino acids increased, the α-helix secondary structure became more stable. For example, seven amino acid length peptides are too short to form an α-helix secondary structure, so they mainly represent a random coil structure (Figure S1A). In contrast, the 14 and 21 amino acid length peptides can form an α-helix secondary structure, but the helicity of the 14 amino acid length peptide is lower than that of the 21 amino acid length peptides (Figure S1B,C). By mutating the polar amino acid (E, Glu) to a hydrophobic amino acid (I, Ile), the same hydrophobicity for each peptide candidate was increased (1.143) for more hydrophobic interactions with PDMS. To minimize the mass effect, the mutation was performed in amino acids that have a similar molecular weight (Glu: 129.12 g/mol and Ile: 113.16 g/mol) per seven amino acids.

Since isoleucine was substituted for glutamic acid, the hydrophobicity was expected to increase, along with the net charge of the peptide, as a nonpolar amino acid was substituted with a negatively charged amino acid. To confirm whether hydrophobicity can be modulated by isoleucine mutation, HPLC was utilized. Figure 1A shows the hydrophobicity change of peptides after mutation measured by HPLC, which can be compared with the hydrophobicity based on retention time. The HPLC retention time measured by HPLC and the theoretical hydrophobicity had a similar tendency, which implies that our peptide candidate is properly constructed (Figure S2).

Development of a PDMS-Coated Matrix for the Study of Hydrophobic Interactions. To measure the hydrophobic interaction between peptides and PDMS, an inorganic solid matrix that consists of PDMS-coated TiO_2 for laser desorption/ionization and hydrophobic interaction with peptides was developed. TiO_2 nanoparticles are used due to their efficiency in the ionization and desorption process of peptides by transferring the charge and energy from a laser to peptides. To observe the binding effect between hydrophobic surfaces and peptides, PDMS was thinly coated onto TiO_2 nanoparticles at a 1.5 nm depth by the thermal deposition
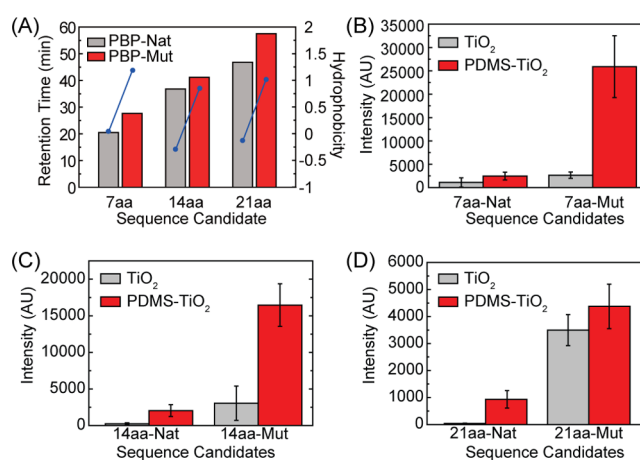

Figure 1. Affinity of hydrophobic modulated peptides to the surface-modified solid matrix using SALDI-MS, whose signal intensity represents the interaction strength which increases depending on the binding affinity. (A) Hydrophobicity measured by HPLC retention time and theoretical hydrophobicity. (B-D) Analysis of SALDI-TOF MS using the TiO_2-based matrix in hydrophobicity dependence. Peptide's mass is (B) <1000 Da (PBP-7aa), (C) >1000 Da (PBP-14aa), and (D) >2000 Da (PBP-21aa).

method. It is important to coat a thin PDMS layer because the energy must be transferred from the TiO_2 nanoparticles. If the thickness of the PDMS layer is >4 nm, the efficiency of energy transfer decreases rapidly. To confirm the surface properties of PDMS-coated TiO_2 nanoparticles, transmission electron microscopy (TEM), Fourier transform infrared (FT-IR) spectroscopy, UV−vis absorption, and X-ray diffraction patterns were measured (Figure S3). The TEM images indicated a thin layer of PDMS with 1.5 nm adsorbed onto the TiO_2 nanoparticle surface (Figure S3B). These data represent local geometric information; the size of the bare TiO_2 nanoparticle was around 15 nm and that of the PDMS-coated TiO_2 nanoparticle was around 18−20 nm due to a thin PDMS layer of 1.5 nm. The functional group of the PDMS-coated TiO_2 nanoparticle surface differs from that of the bare TiO_2 nanoparticle surface. The surface modification of the TiO_2 nanoparticle by PDMS was confirmed by FT-IR spectra, as shown in Figure S3C. The FT-IR spectra of the PDMS-coated TiO_2 nanoparticle surface show sharp peaks at 2964 and 1100 cm^{-1}, corresponding to the asymmetric stretching of CH_3 and Si−O−Si, respectively. The peak at 1261 cm^{-1} is due to the symmetric deformation of the Si−CH_3 frequency of PDMS. The bending peak at 1630 cm^{-1} of H−O−H

corresponds to a hydrophilic surface bare TiO$_2$ nanoparticles, which is absent in the PDMS-coated TiO$_2$ hydrophobic surface. Further, the results of UV−vis absorption spectra (Figure S3D) show that the prepared inorganic matrix absorbs UV light below 390 nm, which deflects that PDMS coating did not affect the optical properties of a TiO$_2$ surface.

To further confirm the hydrophobicity of PDMS-coated TiO$_2$, the water contact angle was measured. The water contact angle of the bare TiO$_2$ nanoparticle surface was difficult to measure due to the hydrophilic properties of TiO$_2$. However, the water contact angle of the PDMS-coated TiO$_2$ nanoparticle surface was measured to be 128.4° (Figure S4B). The modification of the hydrophilic surface of bare TiO$_2$ to PDMS-coated TiO$_2$ caused a hydrophobic surface to be developed. For the solubility check, the bare and PDMS-coated TiO$_2$ nanoparticles were dissolved in DI water. The results showed that the hydrophilic surface of the bare TiO$_2$ nanoparticles became hydrophobic because of the PDMS polymer coating (Figure S4C).

Binding of Modulated Peptides to the PDMS Surface. To study the hydrophobic interaction between peptides and PDMS, the SALDI-TOF simulation was performed using a newly developed inorganic PDMS-coated TiO$_2$ matrix. The signal intensity of all peptide candidates on the PDMS-coated TiO$_2$ matrix was higher than that on the bare TiO$_2$ matrix due to an increase in the hydrophobicity of the matrix. The SALDI-TOF signal intensity indicates the number of peptides bound to the matrix, which reflects a binding affinity with the matrix molecule. The SALDI-TOF signal intensity increases when the polar amino acid is mutated to a hydrophobic amino acid at a similar molecular weight of the peptides. A similar pattern of increasing hydrophobicity in peptides induced by more binding to the PDMS surface was observed with all the three-length candidates, as shown in Figure 1B−D.

In the PBP-7aa candidates with a random coil structure, PBP-7aa-Mut was bound to PDMS 10.5 times more than PBP-7aa-Nat (Figure 1B). Surprisingly, the mutation in just one residue (E to I) highly affected the binding affinity increase. In contrast, PBP-21aa-Mut with a fully α-helix structure bound to PDMS 4.7 times more than PBP-21aa-Nat, despite the mutation of three residues for an increase in hydrophobicity (Figure 1D). In PBP-14aa with partially α-helix and partially random coil structures, mutations increase the binding affinity 8.1 times higher than fully α-helix structures and lower than fully random coil structures. SALDI-TOF results showed the same increase in hydrophobicity in PBP-7aa and PBP-21aa, which had different mutation effects due to the secondary structure of peptides. Our results suggest that the flexibility of random coil structures maximizes the mutation effect for hydrophobic interactions, while the structural stability of α-helix structures has less effect on mutation.

To gain insights into the structural effectiveness of interaction with the hydrophobic surface of PDMS and confirm the correspondence of experimental and theoretical approaches, MD simulations were performed (Figure 2A). Based on the MD simulation results, the analysis of the secondary structure of peptides on PDMS and the calculation of binding affinity between peptides and PDMS were performed. The peptides were quickly adsorbed on the PDMS surface (Figure S6), and the binding energy was calculated using the molecular mechanics Poisson−Boltzmann surface area (MM-PBSA) method. The total binding energy between peptides of different lengths and PDMS increases
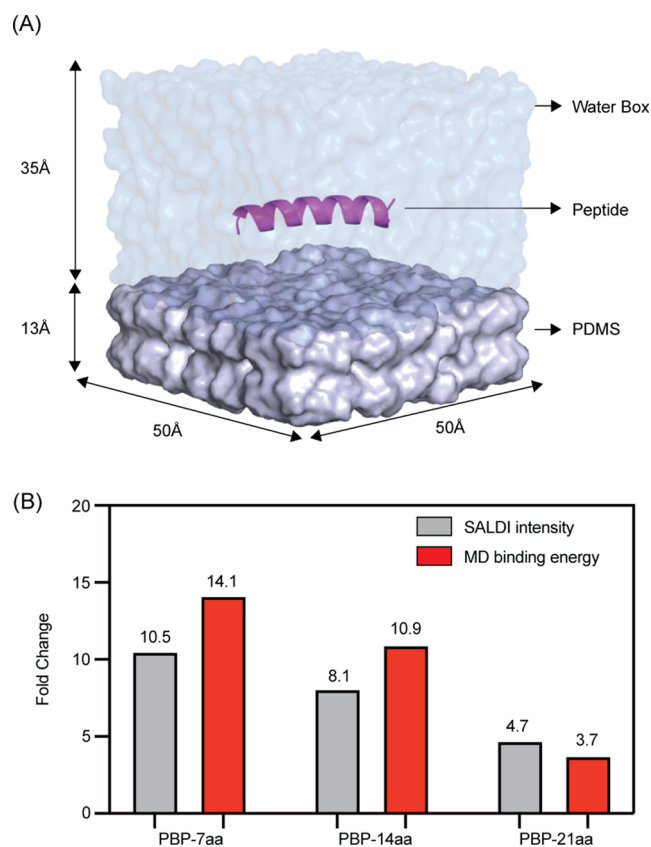

Figure 2. (A) System for simulations mimicking adsorption of modulated peptides. (B) The binding affinity of peptide candidates was calculated with both the experimental method (SALDI-TOF) and theoretical method (MD simulation; binding energy of peptides with the PDMS surface). Fold change is calculated by dividing the intensity of the Mut candidate by the intensity of the Nat candidate.

after mutation from polar amino acid to hydrophobic amino acid (Figure 2B). Through a detailed investigation of the results, it can be deduced that the main driving force of the adsorption is van der Waals interactions as they are consistently increased by increasing the hydrophobicity of the modulated peptides. The van der Waals interaction in total binding energy showed a high energy increase, whereas electrostatic repulsion decreased by mutation from a charged amino acid to a hydrophobic amino acid.

As a result, the SALDI-TOF and MD simulation results correspond in terms of binding affinity between peptides and PDMS (Figure 2B). Like the SALDI-TOF result, the mutation effect was different at the three lengths of a peptide. The seven amino acid length peptides with a random coil structure (PBP-7aa) had the biggest increase in hydrophobic interaction in both experimental and theoretical measurements (10.5 and 13.7 folds, respectively). In contrast, the 21 amino acid length peptides with a fully α-helix structure (PBP-21aa) had the smallest mutation effect in experimental and theoretical measurements (4.7 and 3.8 folds, respectively).

After 500 ns simulations, the positively charged amino acids headed for the solvent interface and did not interact with the PDMS surface in PBP-7aa-Nat and PBP-21aa-Nat. After mutation from a positively charged amino acid to a hydrophobic amino acid, the mutated residue headed for and interacts with the PDMS surface in both PBP-7aa-Mut and PBP-21aa-Mut. However, the conformational change in the
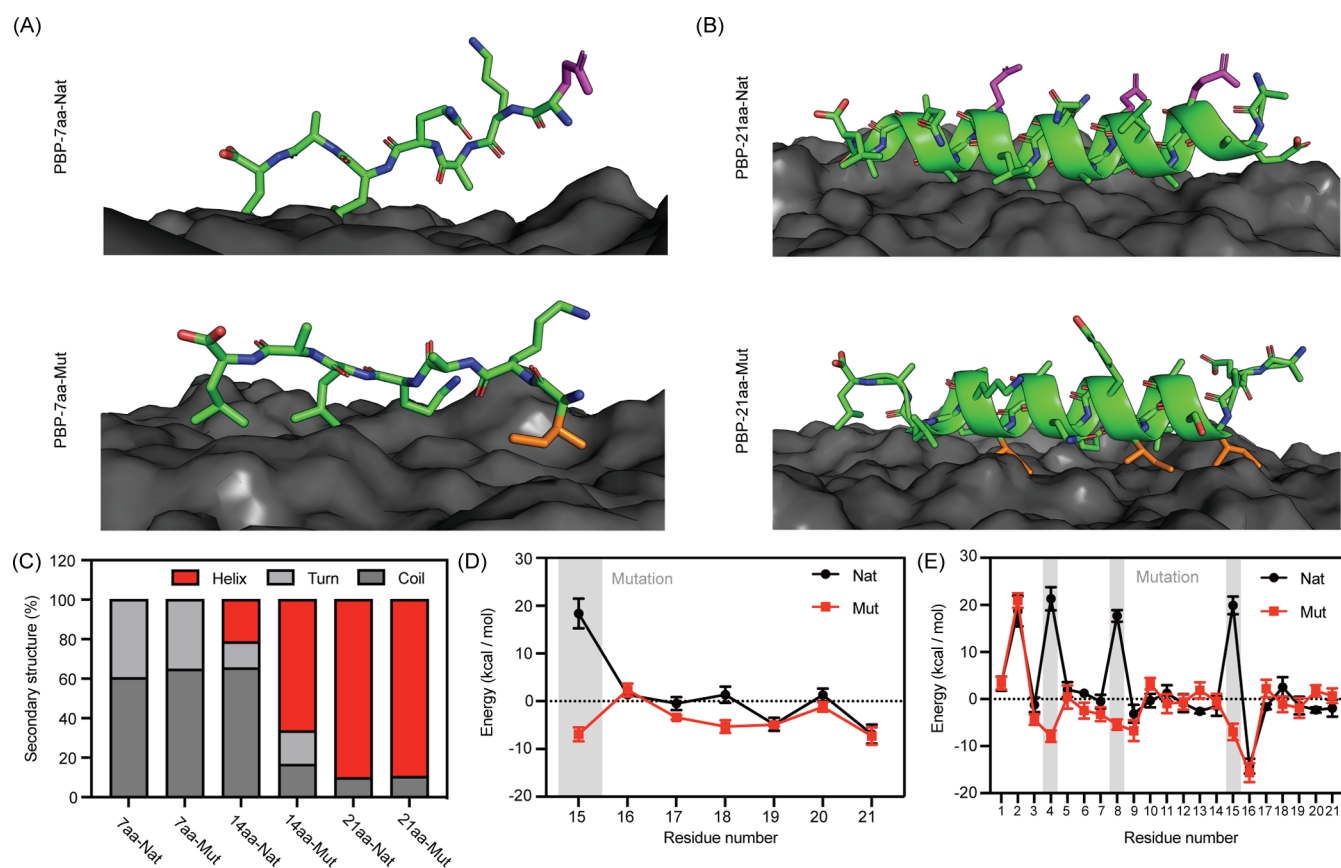
Figure 3. Structural and energetic analyses of peptide adsorption on PDMS via MD simulations. Representative structures of (A) PBP-7aa and (B) PBP-21aa candidates after 500 ns equilibrium simulations. (C) Secondary structure analysis during the last 50 ns simulations. (D,E) Binding energy of each residue in (D) PBP-7aa and (E) PBP-21aa with the PDMS surface before and after mutations.

peptide was different as the secondary structure was either a random coil or an α-helix (Figure 3A,B). In the case of PBP-7aa with a random coil structure, the mutated residue changed the position and increased the binding affinity (Figure 3D,E). In the case of PBP-21aa with an α-helix structure, the entire α-helix structure was rotated for interaction between mutated residues and the PDMS surface (Figure 3B). The interactions between mutated residues and the PDMS surface increased, and the overall interaction network changed (Figure 3E). These differences in interaction network changes after the mutation induced higher binding energy in PBP-7aa than in PBP-21aa.

The secondary structure at each amino acid of six peptide candidates is analyzed using STRIDE software, which is used to determine the secondary structures while considering the hydrogen bond interaction and the dihedral angle of the peptide backbone (Figures 3C and S7). In the case of 7 and 21 amino acid length peptides, they did not exhibit any difference in the secondary structure before and after the mutation of a polar amino acid to a hydrophobic amino acid (a fully random coil or a fully α-helix structure, respectively). The 14 amino acid length peptide and a slightly unfolded α-helix structure showed structural folding to α-helix near the mutated sequence site. These results conclude that more unfolding of the secondary structure caused by a reduction in the number of amino acids maximizes the effect of mutation for increasing the hydrophobic interaction with the PDMS surface. This has been correlated with circular dichroism, which can observe the secondary structure of the modulated peptide. 7aa-Nat and 7aa-Mut were random coils that showed negative ellipticity at 200 nm, while the longer peptides, 14aa and 21aa, showed a significant increase in α-helical propensity, and mutated candidates did not cause a conformational change compared to the native sequence.

■ CONCLUSIONS

The hydrophobic interactions between peptides and hydrophobic solid surfaces were first demonstrated at the atomic level via both experimental and theoretical methods employing a newly developed hydrophobic solid matrix and MD simulations. To control the secondary structure of peptides and hydrophobicity, we made their modulation by changing the length of amino acids and mutating polar amino acids into hydrophobic amino acids. We could decouple the parameters of the hydrophobic effect on a surface with sequence and structure. When the peptide has low structural robustness, the mutation effects are maximized in hydrophobic interactions with the hydrophobic surface, but when the structure is well folded, the hydrophobicity of the interface is less effective than the flexible secondary structure. Our work provides insights into the design or modulation principles of peptide adsorption on the hydrophobic surface of nanomaterials, which may open novel ways for developing innovative biomimetic and biocompatible applications.

ASSOCIATED CONTENT

ⓢ Supporting Information

The Supporting Information is available free of charge at https://pubs.acs.org/doi/10.1021/acsomega.2c03934.

Secondary structure analysis, hydrophobicity of peptides, properties of the PDMS-coated TiO_2 matrix, and experimental data for SALDI-TOF measurements (PDF)

AUTHOR INFORMATION

Corresponding Authors

Wan Soo Yun − *Department of Chemistry, Sungkyunkwan University, Suwon 16419, Republic of Korea;* Email: wsyun87@skku.edu

Young Dok Kim − *Department of Chemistry, Sungkyunkwan University, Suwon 16419, Republic of Korea;* ⓘ orcid.org/0000-0003-1138-5455; Email: ydkim91@skku.edu

Yong Ho Kim − *SKKU Advanced Institute of Nanotechnology (SAINT), Department of Chemistry, and Department of Nano Engineering, Sungkyunkwan University, Suwon 16419, Republic of Korea; Imnewrun Inc., Suwon 16419, Republic of Korea;* ⓘ orcid.org/0000-0002-9106-3298; Email: yhkim94@skku.edu

Authors

Young Hyun No − *SKKU Advanced Institute of Nanotechnology (SAINT), Sungkyunkwan University, Suwon 16419, Republic of Korea;* ⓘ orcid.org/0000-0002-3653-6339

Nam Hyeong Kim − *SKKU Advanced Institute of Nanotechnology (SAINT), Sungkyunkwan University, Suwon 16419, Republic of Korea*

Muhammad Shahzad Zafar − *School of Chemical Engineering, Sungkyunkwan University, Suwon 16419, Republic of Korea; Department of Chemical Engineering, University of Engineering and Technology (Faisalabad Campus), Lahore 54890, Pakistan*

Seon Hwa Park − *Department of Chemistry, Sungkyunkwan University, Suwon 16419, Republic of Korea*

Jaecheol Lee − *School of Pharmacy, Biomedical Institute for Convergence at SKKU (BICS), and Department of Biopharmaceutical Convergence, Sungkyunkwan University, Suwon 16419, Republic of Korea; Imnewrun Inc., Suwon 16419, Republic of Korea*

Heeyeop Chae − *School of Chemical Engineering, Sungkyunkwan University, Suwon 16419, Republic of Korea;* ⓘ orcid.org/0000-0002-6380-0414

Complete contact information is available at:
https://pubs.acs.org/10.1021/acsomega.2c03934

Author Contributions

The manuscript was written through contributions of all authors. All authors have given approval to the final version of the manuscript. Y.H.N., N.H.K., M.S.Z., and S.H.P. contributed equally.

Notes

The authors declare the following competing financial interest(s): Y.H.K. and J.L. are Vice President of Imnewrun INC. and may have competing financial interest. N.H.K. receives research fellowship grant from IMNEWRUN INC.

REFERENCES

(1) Li, Z.; Yin, J.; Gao, C.; Sheng, L.; Meng, A. A Glassy Carbon Electrode Modified with Graphene Oxide, Poly (3, 4-Ethylenedioxythiophene), an Antifouling Peptide and an Aptamer for Ultrasensitive Detection of Adenosine Triphosphate. *Mikrochim. Acta* **2019**, *186*, 90.

(2) Chen, J.; Nugen, S. R. Detection of Protease and Engineered Phage-Infected Bacteria Using Peptide-Graphene Oxide Nanosensors. *Anal. Bioanal. Chem.* **2019**, *411*, 2487−2492.

(3) Meng, F.; Sun, H.; Huang, Y.; Tang, Y.; Chen, Q.; Miao, P. Peptide Cleavage-Based Electrochemical Biosensor Coupling Graphene Oxide and Silver Nanoparticles. *Anal. Chim. Acta* **2019**, *1047*, 45−51.

(4) Kim, J. E.; No, Y. H.; Kim, J. N.; Shin, Y. S.; Kang, W. T.; Kim, Y. R.; Kim, K. N.; Kim, Y. H.; Yu, W. J. Highly Sensitive Graphene Biosensor by Monomolecular Self-Assembly of Receptors on Graphene Surface. *Appl Phys Lett* **2017**, *110* (20), No. 203702.

(5) Ren, T.; Wang, Y.; Yu, Q.; Li, M. Synthesis of Antimicrobial Peptide-Grafted Graphene Oxide Nanosheets with High Antimicrobial Efficacy. *Mater. Lett.* **2019**, *235*, 42−45.

(6) Pramanik, A.; Gates, K.; Gao, Y.; Zhang, Q.; Han, F. X.; Begum, S.; Rightsell, C.; Sardar, D.; Ray, P. C. Composites Composed of Polydopamine Nanoparticles, Graphene Oxide, and E-Poly-L-Lysine for Removal of Waterborne Contaminants and Eradication of Superbugs. *ACS Appl. Nano Mater.* **2019**, *2*, 3339−3347.

(7) Toublan, F. J.-J.; Boppart, S.; Suslick, K. S. Tumor Targeting by Surface-Modified Protein Microspheres. *J. Am. Chem. Soc.* **2006**, *128*, 3472−3473.

(8) Pampaloni, N. P.; Giugliano, M.; Scaini, D.; Ballerini, L.; Rauti, R. Advances in Nano Neuroscience: From Nanomaterials to Nanotools. *Front. Neurol.* **2019**, *12*, 953.

(9) Ligorio, C.; Zhou, M.; Wychowaniec, J. K.; Zhu, X.; Bartlam, C.; Miller, A. F.; Vijayaraghavan, A.; Hoyland, J. A.; Saiani, A. Graphene Oxide Containing Self-Assembling Peptide Hybrid Hydrogels as a Potential 3d Injectable Cell Delivery Platform for Intervertebral Disc Repair Applications. *Acta Biomater.* **2019**, *92*, 92−103.

(10) Yang, Q.; Kaul, C.; Ulbricht, M. Anti-Nonspecific Protein Adsorption Properties of Biomimetic Glycocalyx-Like Glycopolymer Layers: Effects of Glycopolymer Chain Density and Protein Size. *Langmuir* **2010**, *26*, 5746−5752.

(11) Chen, S.; Li, L.; Zhao, C.; Zheng, J. Surface Hydration: Principles and Applications Toward Low-Fouling/Nonfouling Biomaterials. *Polymer* **2010**, *51*, 5283−5293.

(12) Elgersma, A. V.; Zsom, R. L.; Lyklema, J.; Norde, W. Kinetics of Single and Competitive Protein Adsorption Studied by Reflectometry and Streaming Potential Measurements. *Colloids Surf.* **1992**, *65*, 17−28.

(13) Norde, W.; Lyklema, J. The Adsorption of Human Plasma Albumin and Bovine Pancreas Ribonuclease at Negatively Charged Polystyrene Surfaces: I. Adsorption Isotherms. Effects of Charge, Ionic Strength, and Temperature. *J. Colloid Interface Sci.* **1978**, *66*, 257−265.

(14) Meder, F.; Daberkow, T.; Treccani, L.; Wilhelm, M.; Schowalter, M.; Rosenauer, A.; Mädler, L.; Rezwan, K. Protein

Adsorption on Colloidal Alumina Particles Functionalized with Amino, Carboxyl, Sulfonate and Phosphate Groups. *Acta Biomater.* **2012**, *8*, 1221−1229.

(15) Mereghetti, P.; Wade, R. C. Diffusion of Hydrophobin Proteins in Solution and Interactions with a Graphite Surface. *BMC Biophys.* **2011**, *4*, 9.

(16) Moldovan, C.; Thompson, D. Molecular Dynamics of the "Hydrophobic Patch" That Immobilizes Hydrophobin Protein HFBII on Silicon. *J. Mol. Model.* **2011**, *17*, 2227−2235.

(17) Liu, Y.; Wu, M.; Feng, X.; Shao, X.; Cai, W. Adsorption Behavior of Hydrophobin Proteins on Polydimethylsiloxane Substrates. *J. Phys. Chem. B* **2012**, *116*, 12227−12234.

(18) Zhao, D.; Li, L.; He, D.; Zhou, J. Molecular Dynamics Simulations of Conformation Changes of HIV-1 Regulatory Protein on Graphene. *Appl. Surf. Sci.* **2016**, *377*, 324−334.

(19) Quan, X.; Liu, J.; Zhou, J. Multiscale Modeling and Simulations of Protein Adsorption: Progresses and Perspectives. *Curr. Opin. Colloid Interface Sci.* **2019**, *41*, 74−85.

(20) Peng, C.; Liu, J.; Zhao, D.; Zhou, J. Adsorption of Hydrophobin on Different Self-Assembled Monolayers: The Role of the Hydrophobic Dipole and the Electric Dipole. *Langmuir* **2014**, *30*, 11401−11411.

(21) No, Y. H.; Kim, N. H.; Gnapareddy, B.; Choi, B.; Kim, Y.-T.; Dugasani, S. R.; Lee, O.-S.; Kim, K.-H.; Ko, Y.-S.; Lee, S.; Lee, S. W.; Park, S. H.; Eom, K.; Kim, Y. H. Nature-Inspired Construction of Two-Dimensionally Self-Assembled Peptide on Pristine Graphene. *J Phys Chem Lett* **2017**, *8* (16), 3734−3739.

(22) Zhou, H.-X.; Dill, K. A. Stabilization of Proteins in Confined Spaces. *Biochemistry* **2001**, *40*, 11289−11293.

(23) Mittal, J.; Best, R. B. Thermodynamics and Kinetics of Protein Folding under Confinement. *Proc. Natl. Acad. Sci. U.S.A.* **2008**, *105*, 20233−20238.

(24) Binazadeh, M.; Zeng, H.; Unsworth, L. Effect of Peptide Secondary Structure on Adsorption and Adsorbed Film Properties on End-Grafted Polyethylene Oxide Layers. *Acta Biomater.* **2014**, *10*, 56−66.

(25) Barreto, M. S. C.; Elzinga, E. J.; Alleoni, L. R. F. The Molecular Insights into Protein Adsorption on Hematite Surface Disclosed by in-Situ Atr-Ftir/2d-Cos Study. *Sci. Rep.* **2020**, *10*, 13441.

(26) Kim, N. H.; Choi, H.; Shahzad, Z. M.; Ki, H.; Lee, J.; Chae, H.; Kim, Y. H. Supramolecular Assembly of Protein Building Blocks: from Folding to Function. *Nano Convergence* **2022**, *9*, 4.

(27) Sethuraman, A.; Belfort, G. Protein Structural Perturbation and Aggregation on Homogeneous Surfaces. *Biophys. J.* **2005**, *88*, 1322−1333.

(28) Danilov, V.; Wagner, H. E.; Meichsner, J. Modification of Polydimethylsiloxane Thin Films in H2 Radio-Frequency Plasma Investigated by Infrared Reflection Absorption Spectroscopy. *Plasma Process. Polym.* **2011**, *8*, 1059−1067.

(29) Guo, J.; Yao, X.; Ning, L.; Wang, Q.; Liu, H. The Adsorption Mechanism and Induced Conformational Changes of Three Typical Proteins with Different Secondary Structural Features on Graphene. *RSC Adv.* **2014**, *4*, 9953−9962.

(30) Raffaini, G.; Ganazzoli, F. Protein Adsorption on a Hydrophobic Surface: A Molecular Dynamics Study of Lysozyme on Graphene. *Langmuir* **2010**, *26*, 5679−5689.

(31) Hosseinpour, S.; Roeters, S. J.; Bonn, M.; Peukert, W.; Woutersen, S.; Weidner, T. Structure and Dynamics of Interfacial Peptides and Proteins from Vibrational Sum-Frequency Generation Spectroscopy. *Chem. Rev.* **2020**, *120*, 3420−3465.

(32) Ye, S.; Majumdar, P.; Chisholm, B.; Stafslien, S.; Chen, Z. Antifouling and Antimicrobial Mechanism of Tethered Quaternary Ammonium Salts in a Cross-Linked Poly(Dimethylsiloxane) Matrix Studied Using Sum Frequency Generation Vibrational Spectroscopy. *Langmuir* **2010**, *26*, 16455−16462.

(33) Huang, J.; Rauscher, S.; Nawrocki, G.; Ran, T.; Feig, M.; de Groot, B. L.; Grubmüller, H.; MacKerell, A. D. CHARMM36m: An Improved Force Field for Folded and Intrinsically Disordered Proteins. *Nat. Methods* **2017**, *14*, 71−73.

(34) Bahar, I.; Zuniga, I.; Dodge, R.; Mattice, W. L. Conformational Statistics of Poly(Dimethylsiloxane). 1. Probability Distribution of Rotational Isomers from Molecular Dynamics Simulations. *Macromolecules* **1991**, *24*, 2986−2992.